MODELING THE IUE NOISE FUNCTION

C. M. Urry, M. J. Bergoffen and R. A. Edelson

ABSTRACT

In order to understand the noise function of the *IUE* data, we have modeled its behavior at 40 wavelength bins, in ~300 low-dispersion data files from three cameras. We model the noise as a function of four parameters: flux, wavelength, camera, and LBL (line-by-line) file format. This model is presently being incorporated into the GEX (Gaussian Extraction) routines in weighting the cross-dispersion fits, testing data points for possible rejection, and producing an output error vector.

I. INTRODUCTION

We have studied more than 300 *IUE* images in an effort to quantify the relation between the signal in a given pixel and the expected associated noise. The motivation for this work was the development of the GEX program (Urry and Reichert 1988), an improved spectral extraction routine. In brief, GEX extracts spectra from *IUE* images using fitted Gaussian profiles in the cross-dispersion direction. The noise model allows us to weight these fits, to reject outlying points, and to associate an error vector with each flux vector. Other applications of this model are also possible. For instance, it can provide the basis for identification of cosmic ray hits, allowing them to be flagged and disregarded during the extraction process.

The noise in *IUE* data does not behave like that in conventional photon-counting noise. For many spectroscopy systems (*e.g.*, radio and millimeter-wave spectrometers, sky-limited CCD spectrographs, *etc.*), the noise behaves in a Gaussian fashion. For these systems, it is usually possible to estimate the uncertainty directly from the data, because Gaussian noise is well-behaved and easily modeled. By contrast, in the *IUE* spectrographs, the noise behaves in a non-Gaussian fashion (Bohlin *et al.* 1980, Kinney *et al.* 1988), and is not well described or understood. From the standard IUESIPS processing, *IUE* astronomers are given only the epsilon vector, a crude noise estimate that declares data either "good" or one of a few flavors of "bad."

Kinney *et al.* (1988) showed that the noise in *IUE* images was a simple linear function of flux, with slightly different constants for each camera or LBL-format. From only three wavelength bins per spectrum, they also concluded the wavelength dependence was linear.

In this paper, we carry this work further, using a larger sample of images and many more wavelength bins per spectrum, to derive a model of the *IUE* noise as a function of flux, wavelength, camera, and LBL format. This procedure is described in the next section. We then discuss these results and compare them with those of Kinney *et al.* in § III. Finally, the implementation of this noise model in the GEX routines is addressed in § IV.

II. PROCEDURE

Our method of deriving the *IUE* noise function is similar to that of Kinney *et al.* (1988). We estimate the noise by measuring the distribution of observed fluxes (F_j) in regions over which the change in wavelength is small and the spread in the distribution of flux numbers is caused only by measurement noise. This means the measurements must be restricted to regions sufficiently far from the signal (spectrum) so that it makes effectively no contribution to the spread. For each *IUE* camera (SWP, LWR, or LWP) and number of lines in the LBL file (55 or 110, depending on processing date), we studied background regions in ~40-130 images, with a wide range of flux levels and exposure times. There were five camera/file format combinations: 1) SWP/110-LBL files (39 files); 2) SWP/55-LBL files (131 files); 3) LWP/110-LBL files (34 files); 4) LWP/55-LBL files (44 files); and 5) LWR/55-LBL files (62 files). The relatively small number of LWR/110-LBL images were omitted from consideration.

As a first step, we pre-filtered the data using the program MEDIAN. This stand-alone IDL program, written by Edelson and Bergoffen, uses a median filtering technique to identify cosmic ray hits. Affected pixels are flagged in the epsilon array but the data themselves are not altered. These data as well as others with bad epsilon values, were excluded from further analysis, since GEX and other programs use the epsilon array to eliminate flagged data from the extraction process.

Background regions were defined to be 10 (18) lines on either side of the spectrum, separated from the central line by 5 (10) lines; numbers refer to 55-LBL (110-LBL) files. Each background swath was further divided into 20 contiguous segments of equal extent in wavelength. For the LW and SW cameras, the final background patches were ~55 Å and ~40 Å long, respectively, or about 10 by 10 (10 by 20) pixels.

For a particular (*ith*) image, the mean flux ($F_i(\lambda)$) at wavelength λ was calculated for each background patch and the noise ($\sigma_i(\lambda)$) was defined as square-root of the variance with respect to the mean in that patch:

$$F_i(\lambda) = \frac{1}{N} \sum_{j=1}^{N} F_j, \tag{1}$$

and

$$\sigma_i(\lambda)^2 = \frac{1}{N} \sum_{j=1}^{N} (F_j - F_i(\lambda))^2. \tag{2}$$

At each wavelength the data from both sides of the spectrum were combined to form one ($F_i(\lambda)$, $\sigma_i(\lambda)$) pair per wavelength bin per spectrum. The calculation was repeated for every image in a given camera/LBL-format set and the resulting ($F_i(\lambda)$, $\sigma_i(\lambda)$) data pairs were used as input data for the noise model.

We find that the noise is well-described by a linear function of both flux and

wavelength (see Figures 1-6):

$$\sigma(F,\lambda) = m(\lambda) \cdot F + b(\lambda), \tag{3}$$

where

$$m(\lambda) = A \cdot \lambda + B, \tag{4}$$

and

$$b(\lambda) = C \cdot \lambda + D. \tag{5}$$

This confirms the findings of Kinney *et al.* (1988). Equations 3–5 can be combined to give:

$$\sigma(F,\lambda) = A \cdot \lambda \cdot F + B \cdot F + C \cdot \lambda + D. \tag{6}$$

The model fits the ($F_i(\lambda)$, $\sigma_i(\lambda)$) data to determine the constants A, B, C, and D for each camera/LBL-format.

Our approach was to fit the ($F_i(\lambda)$, $\sigma_i(\lambda)$) data to determine $m(\lambda)$ and $b(\lambda)$ in equation (3) for each wavelength bin in a given camera/file format combination. The standard RDAF subroutine LINFIT was used to determine the slope ($m(\lambda)$) and intercept ($b(\lambda)$) of the relation, and their associated errors. Figure 1 shows typical fits at three different wavelength bins, 2286 Å, 2623 Å, and 2903 Å, for the LWP/55-LBL images. These data are well described by a straight line. The data in Figure 1 are listed in Table 1.

The results of the fits to equation (3) for the SWP/110, SWP/55, LWP/110, LWP/55, and LWR/55 combinations are presented in Tables 2–6, respectively. These data show that $m(\lambda)$ and $b(\lambda)$ are linear functions of λ, which indicates that equation (6) is a valid description of the functional dependence of noise on flux and wavelength. (That is, the inclusion of higher order terms would not significantly improve the fit and is therefore not warranted.) To solve for the constants A, B, C, and D in equations (4) and (5) we again used LINFIT, this time weighting values of $m(\lambda)$ and $b(\lambda)$ by the inverse of the square of the uncertainties listed in Tables 2–6. The data and best linear fits are shown in Figures 2–6. Each point with error bars represents ~50 background measurements.

The final results of our noise model, fits to Equation (6) for each camera/LBL format, are presented in Table 7. The noise σ (in FN) associated with a flux F (in FN) at a wavelength λ (in Å) for any pixel in any camera can be predicted directly from this table using Equation (6). One simply chooses the parameters A, B, C and D appropriate to the camera/LBL file format of interest from Table 7, and then applies equation (6) to determine $\sigma(F,\lambda)$.

III. DISCUSSION

For the SWP/110 combination (Figure 2 and Table 2), one point at ~1430 Å is clearly anomalous. We went back to the images to try to discover the origin of this discrepant point, and we found that for some reason the noise at that wavelength was simply higher on one side the the spectrum; the other side was "normal." Therefore, in fitting for $m(\lambda)$ and $b(\lambda)$, this point was ignored. This made only a very slight difference to the derived parameters.

We can compare our derived slopes and intercepts for $\sigma(F)$ with those of Kinney *et al.* (1988), at the three wavelengths measured in that paper. These are given in Table 8. It is interesting to note that the LWR camera differs from the LWP and SWP cameras in its noise characteristics: The dependence of $m(\lambda)$ and $b(\lambda)$ on wavelength is of opposite sign for the LWR camera. This result is in contrast to that of Kinney *et al.*, which found that there was no wavelength dependence.

IV. APPLICATION

This noise model is now being implemented in the GEX spectral extraction routines. As described by Urry and Reichert (1988), GEX extracts spectra from *IUE* images using fitted Gaussian profiles in the cross-dispersion direction. Previously the fits were not weighted; we are now implementing the noise model described above in the GEX routines in part to weight points in the cross-dispersion fits. (The weights are inversely proportional to the variance σ^2.)

In GEX, background-subtracted points in the central signal region are fitted with a Gaussian (now weighting by $1/\sigma^2$). In order not to bias the fits, we must calculate σ according to the value of F in the model rather than the data (Horne 1986). Therefore the fitting is done iteratively: first we use the data values to calculate σ, then we find the weighted best-fit Gaussian, then we use that model to re-calculate σ, then we re-fit, and so on. Experience shows that the fit converges after a few iterations for even the poorest exposures.

Noise estimates from the model are also used to determine rejection of outlying points. Previously, as described by Urry and Reichert (1988), points lying further than $\sim 2\sigma$ from the best-fit cross-dispersion profile were rejected and the profile re-calculated. The value of σ used was just the standard deviation of the background points about the linear background fit. Now GEX uses the value of σ appropriate to each point in the background and signal regions, calculated from the flux and wavelength at that point according to Table 7.

The noise model is also used to generate an uncertainty in the final flux value obtained from GEX. This is less straightforward than the two applications described above since the flux is proportional to the area under the background-subtracted Gaussian curve, and each point on that curve has its own σ.

V. REFERENCES

Barylak, M. 1982, *IUE Newsletter*, **21**, 55.

Bohlin, R. C., Holm, A. V., Savage, B. D., Snijders, M. A. J., and Sparks, W. M. 1980, *Astr. Ap.*, **85**, 1.

Horne, K. 1986, *P. A. S. P.*, **98**, 609.

Kinney, A. L., Bohlin, R. C., and Neill, J. D. 1988, *IUE Newsletter*, **35**. 114.

Urry, C. M., and Reichert, G. 1988, *IUE Newsletter*, **34**, 95.

Table 1

LWP Data

LWP	$F(2286)$	$\sigma(2286)$	$F(2623)$	$\sigma(2623)$	$F(2903)$	$\sigma(2903)$
1353	1547.6	843.72	1564.4	453.05	1504.4	313.40
1414	2890.4	796.51	2670.1	446.87	2755.4	320.08
1490	2564.1	768.94	2549.8	579.84	2307.3	302.57
1493	2303.1	817.46	2307.7	484.90	2151.9	501.78
1550	4556.9	1028.0	4631.3	675.09	4995.8	418.84
1565	2727.6	672.61	2639.6	385.81	2857.1	350.11
1579	4067.9	898.20	4078.0	660.80	4333.4	398.15
1603	7604.0	1009.9	7591.2	740.31	8094.7	638.40
1630	3486.3	935.19	3347.3	619.29	3452.1	353.10
1647	6635.5	1108.5	7020.0	892.58	7162.5	704.79
1649	7485.3	1209.2	7284.1	826.20	7665.7	537.43
1404	5468.9	1108.0	5914.8	708.27	5855.6	587.85
1371	3021.7	780.52	2679.0	444.75	2654.7	306.39
1744	3158.3	826.49	3022.2	519.48	3278.2	387.01
1752	12227.	1663.5	12653.	1245.1	12975.	711.47
1797	2915.8	948.88	2797.7	550.28	2846.1	340.13
1798	2876.7	940.92	2871.7	519.07	2963.3	302.53
1888	3664.5	976.61	3654.3	577.39	3701.4	379.62
1910	2857.4	861.98	2934.3	558.46	2840.7	347.10
2399	5062.0	917.03	4659.1	645.11	4723.4	586.21
2417	12068.	1832.0	12300.	1180.4	12684.	726.91
2525	5002.9	1000.6	4861.4	641.39	4810.8	441.34
2537	12343.	1840.7	13140.	1270.4	13158.	730.21
2541	10806.	1359.6	10588.	895.30	10853.	586.74
2827	4337.9	940.78	4034.0	632.70	4005.9	360.98
2836	3782.3	896.41	3483.4	525.92	3578.2	335.54
3287	9696.4	1181.8	9883.3	913.08	10247.	505.86
3417	14019.	1747.7	14187.	1241.6	14377.	709.30
3525	5951.7	946.79	5570.9	614.25	5545.1	447.86
4265	7238.2	1259.2	6780.9	781.20	6841.7	528.91
4680	4923.6	887.41	4844.7	679.34	4970.8	493.50
5378	6378.9	1106.4	6046.8	747.59	6076.0	497.68
5397	1641.9	628.15	1241.9	326.31	1484.5	276.17
6169	8111.3	1173.8	8229.3	804.72	8284.0	564.05
6178	1480.3	603.85	1279.7	362.22	1153.3	206.06
6179	4753.1	881.49	4547.1	601.47	4558.0	394.38
6180	3935.8	793.20	3637.8	597.98	3709.0	373.49
6202	4460.3	706.39	4440.1	512.97	4410.1	435.15
6203	5570.8	970.15	5404.5	689.79	5495.0	513.00
6215	4201.3	713.89	4163.9	509.45	4118.4	310.38
6216	4635.1	907.20	4370.1	617.02	4285.8	362.68
6246	4688.9	1063.4	4067.7	575.13	4066.3	368.39
6247	4414.3	802.81	4090.7	501.90	4111.5	346.32
6262	6448.7	994.72	6271.4	703.79	6307.0	479.18

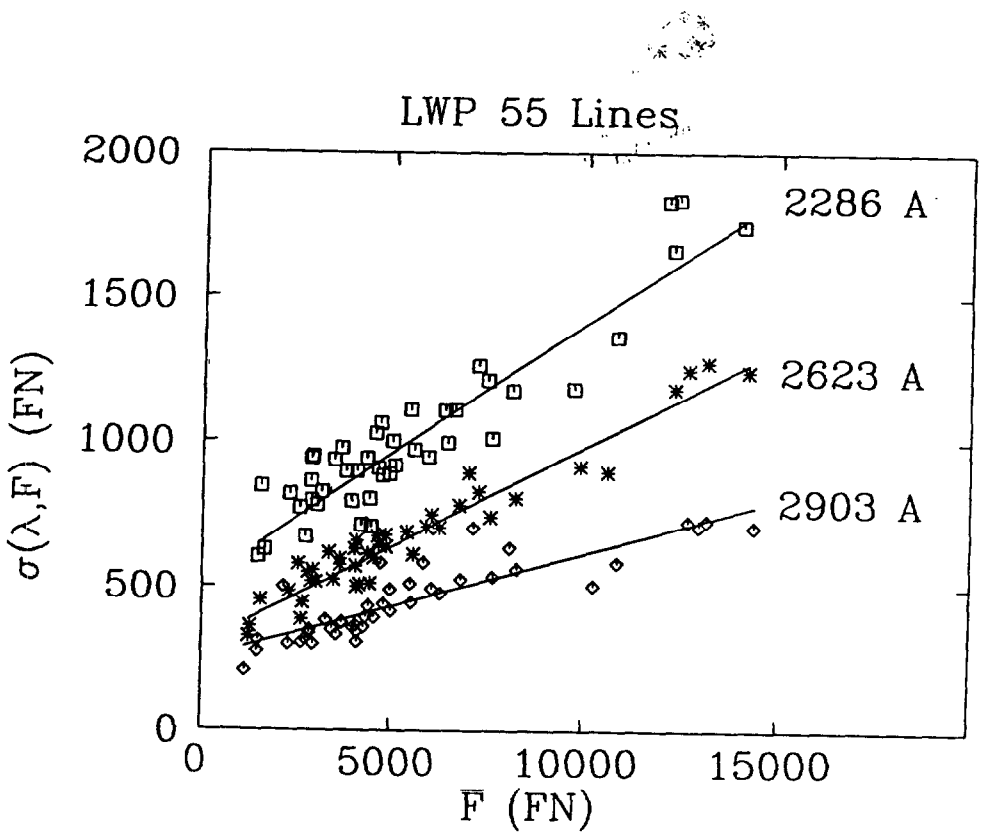

Figure 1 – Plot of σ as a function of F for the LWP/55 data.

Table 2

SWP 110-LBL (39 files)

λ	$b(\lambda)$	$m(\lambda)$
1251.0	241.44 ± 18.28	0.05452 ± 0.00432
1287.6	253.57 ± 25.47	0.05568 ± 0.00607
1324.1	238.35 ± 17.62	0.04946 ± 0.00420
1360.9	245.16 ± 26.90	0.04739 ± 0.00641
1397.5	224.13 ± 17.28	0.05419 ± 0.00411
1434.1	205.29 ± 32.58	0.06598 ± 0.00777
1470.8	179.09 ± 32.98	0.05512 ± 0.00785
1507.5	173.29 ± 31.80	0.05601 ± 0.00760
1544.1	159.33 ± 26.32	0.05562 ± 0.00630
1580.8	182.73 ± 14.79	0.04071 ± 0.00354
1617.3	165.61 ± 11.33	0.03871 ± 0.00274
1654.0	156.13 ± 15.17	0.03767 ± 0.00372
1690.7	150.22 ± 11.78	0.03491 ± 0.00293
1727.3	123.56 ± 12.35	0.03772 ± 0.00311
1764.0	120.02 ± 9.72	0.03109 ± 0.00249
1800.6	119.16 ± 12.15	0.03549 ± 0.00314
1837.2	96.66 ± 19.00	0.03890 ± 0.00497
1873.9	76.38 ± 21.12	0.03990 ± 0.00553
1910.5	61.98 ± 24.66	0.04522 ± 0.00641
1947.2	233.37 ± 87.37	0.13064 ± 0.02225

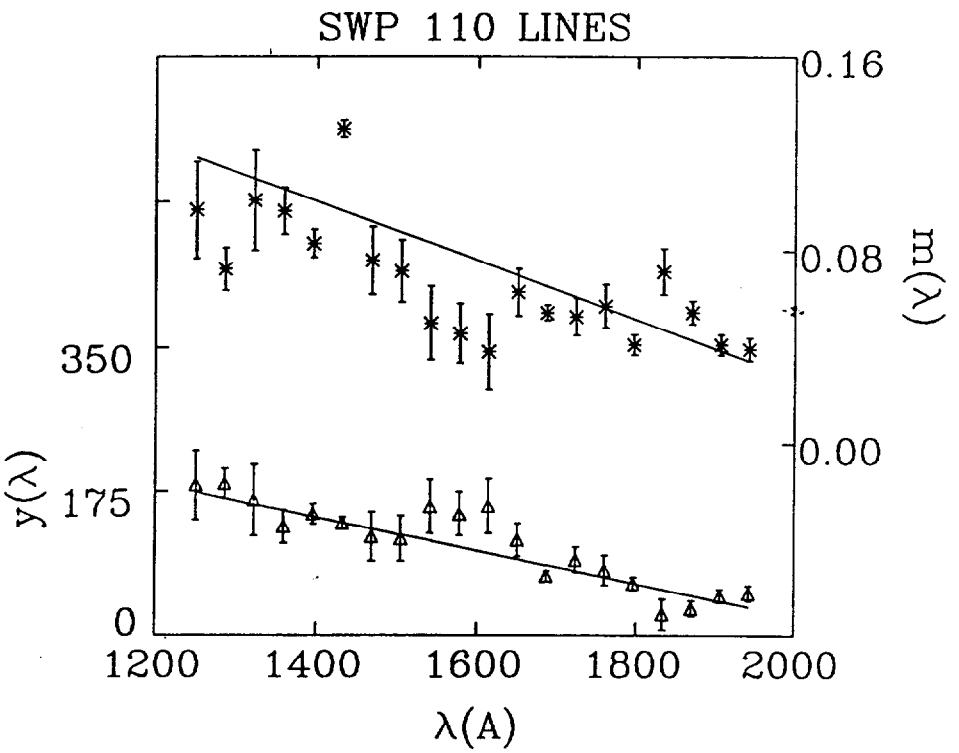

Figure 2 – Plot of σ as a function of fitting parameters $m(\lambda)$ and $b(\lambda)$ for the SWP/110 data.

Table 3

SWP 55-LBL (131 files)

λ	$b(\lambda)$	$m(\lambda)$
1250.2	182.91 ± 42.05	0.09677 ± 0.01990
1286.5	184.61 ± 18.32	0.07243 ± 0.00875
1322.9	164.53 ± 43.39	0.10067 ± 0.02064
1359.3	132.55 ± 20.27	0.09627 ± 0.00956
1395.7	147.97 ± 12.23	0.08296 ± 0.00576
1432.2	136.68 ± 7.41	0.13008 ± 0.00356
1468.6	120.42 ± 29.86	0.07585 ± 0.01388
1505.0	117.94 ± 27.50	0.07144 ± 0.01287
1541.3	156.55 ± 32.53	0.05016 ± 0.01522
1577.7	147.72 ± 26.25	0.04593 ± 0.01231
1614.2	157.07 ± 32.92	0.03826 ± 0.01564
1650.6	116.35 ± 19.94	0.06287 ± 0.00963
1687.0	72.17 ± 6.55	0.05465 ± 0.00316
1723.5	92.11 ± 15.44	0.05295 ± 0.00752
1759.9	79.19 ± 18.02	0.05726 ± 0.00887
1796.3	62.68 ± 8.50	0.04143 ± 0.00431
1832.6	25.38 ± 18.64	0.07157 ± 0.00944
1869.0	32.44 ± 9.36	0.05471 ± 0.00477
1905.4	47.76 ± 8.22	0.04139 ± 0.00421
1941.9	51.00 ± 9.36	0.03953 ± 0.00475

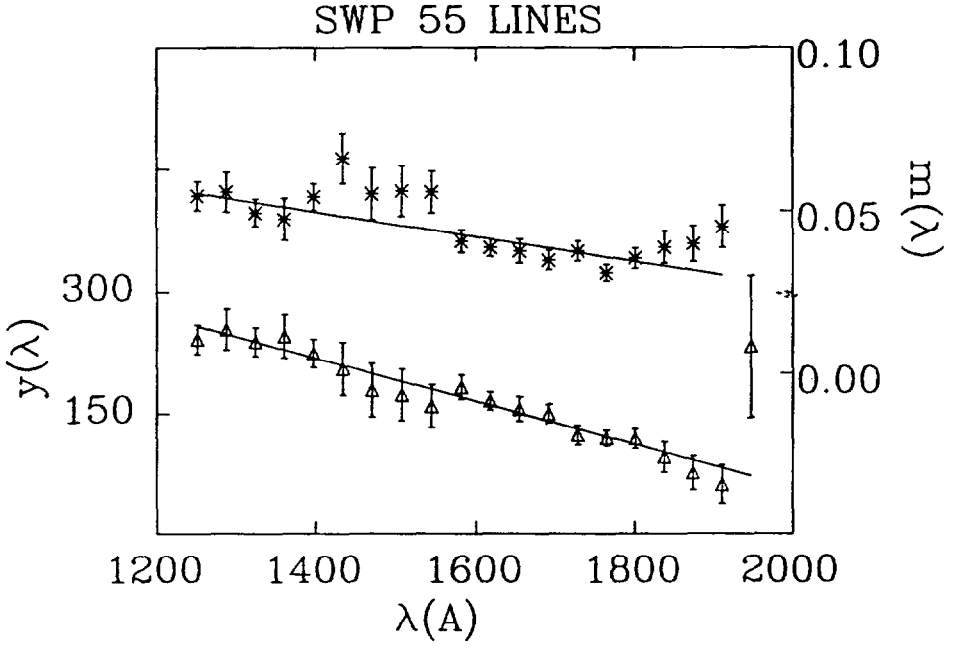

Figure 3 – Plot of σ as a function of fitting parameters $m(\lambda)$ and $b(\lambda)$ for the SWP/55 data.

Table 4

LWP 110-LBL (34 files)

λ	$b(\lambda)$	$m(\lambda)$
1950.6	465.80 ± 37.86	0.14972 ± 0.01233
2006.0	439.55 ± 19.85	0.12716 ± 0.00648
2062.2	343.70 ± 10.37	0.12916 ± 0.00340
2118.2	377.62 ± 33.81	0.12388 ± 0.01119
2174.4	339.27 ± 18.28	0.12965 ± 0.00598
2230.4	265.20 ± 30.18	0.13423 ± 0.00998
2286.4	293.64 ± 14.29	0.10842 ± 0.00474
2342.6	298.25 ± 13.02	0.09320 ± 0.00433
2398.6	277.81 ± 10.85	0.12930 ± 0.00374
2454.8	236.21 ± 6.78	0.08922 ± 0.00229
2510.8	218.50 ± 21.15	0.08321 ± 0.00716
2567.0	197.46 ± 13.49	0.07519 ± 0.00460
2623.0	173.11 ± 10.88	0.07200 ± 0.00371
2679.2	128.48 ± 16.58	0.06962 ± 0.00566
2735.2	113.70 ± 6.84	0.06159 ± 0.00234
2791.2	112.95 ± 8.06	0.05207 ± 0.00274
2847.4	121.98 ± 24.95	0.05321 ± 0.00841
2903.4	113.00 ± 9.07	0.04485 ± 0.00304
2959.6	98.58 ± 8.36	0.04270 ± 0.00276
3015.6	82.51 ± 8.62	0.04894 ± 0.00281

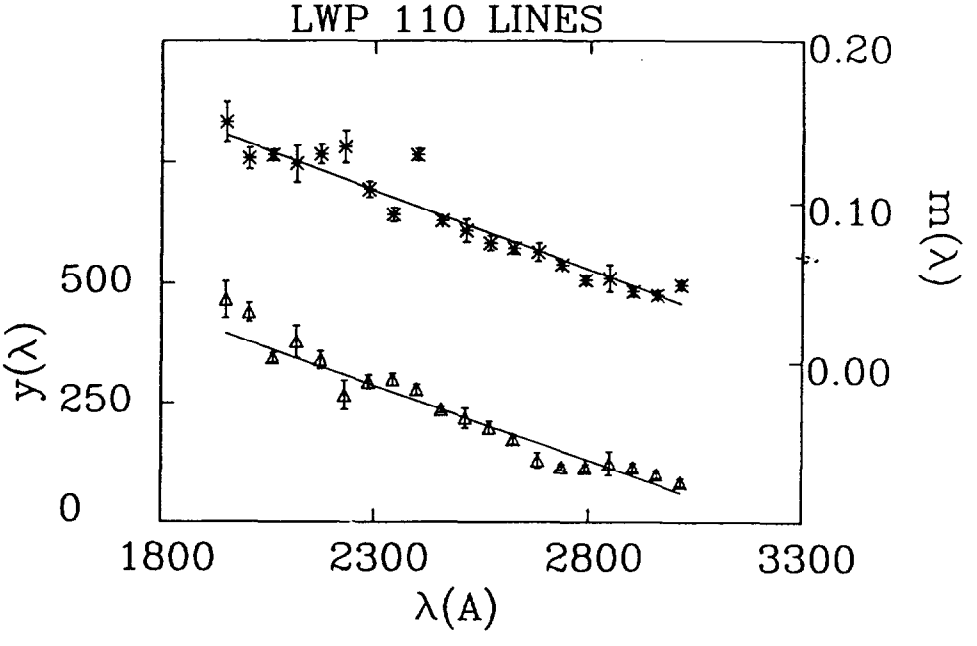

Figure 4 – Plot of σ as a function of fitting parameters $m(\lambda)$ and $b(\lambda)$ for the LWP/110 data.

Table 5

LWP 55-LBL (44 files)

λ	$b(\lambda)$	$m(\lambda)$
1950.6	828.52 ± 46.02	0.09174 ± 0.00737
2006.0	679.60 ± 32.84	0.10741 ± 0.00524
2062.1	629.38 ± 32.74	0.10334 ± 0.00526
2118.2	595.76 ± 63.40	0.10958 ± 0.01012
2174.3	581.12 ± 32.69	0.09615 ± 0.00527
2230.4	450.34 ± 27.69	0.10387 ± 0.00445
2286.4	514.17 ± 34.98	0.08900 ± 0.00568
2342.6	485.96 ± 32.99	0.08421 ± 0.00529
2398.6	478.08 ± 39.96	0.08733 ± 0.00651
2454.7	449.21 ± 24.28	0.07610 ± 0.00392
2510.8	390.75 ± 18.74	0.07041 ± 0.00304
2566.9	373.18 ± 20.19	0.06349 ± 0.00327
2623.0	300.96 ± 17.61	0.06794 ± 0.00286
2679.1	282.14 ± 21.23	0.05241 ± 0.00345
2735.1	251.83 ± 17.66	0.05311 ± 0.00286
2791.2	228.14 ± 15.39	0.04726 ± 0.00249
2847.3	218.06 ± 12.22	0.04384 ± 0.00197
2903.4	247.79 ± 18.62	0.03682 ± 0.00297
2959.5	214.07 ± 13.16	0.03911 ± 0.00207
3015.5	186.59 ± 12.05	0.03856 ± 0.00188

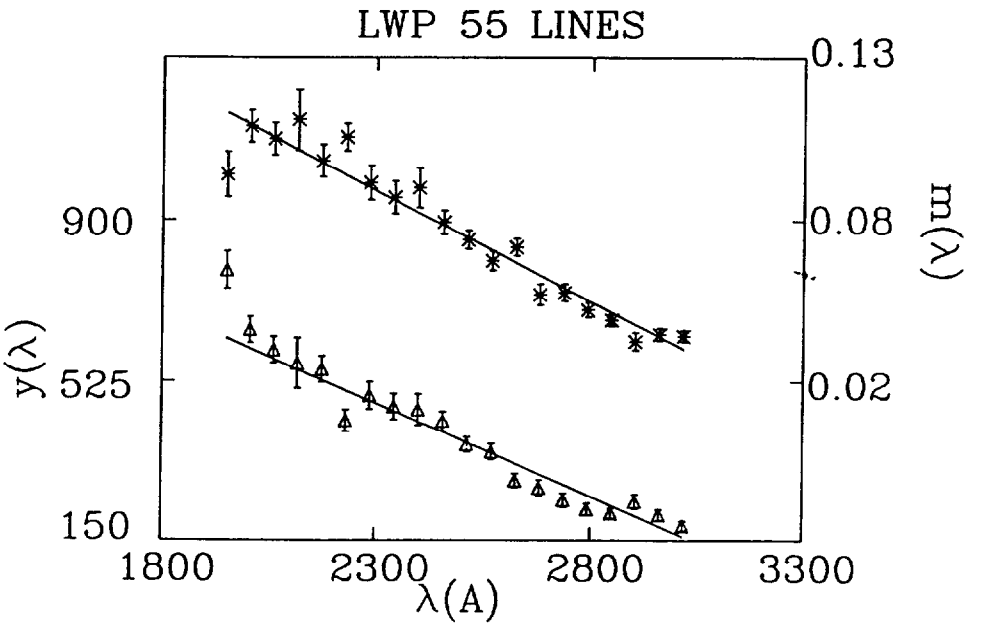

Figure 5 – Plot of σ as a function of fitting parameters $m(\lambda)$ and $b(\lambda)$ for the LWP/55 data.

Table 6

LWR 55-LBL (62 files)

λ	$b(\lambda)$	$m(\lambda)$
1951.3	320.78 ± 35.10	0.05043 ± 0.00315
2007.2	340.95 ± 34.23	0.05364 ± 0.00310
2064.1	319.97 ± 32.55	0.05599 ± 0.00293
2120.7	397.03 ± 36.21	0.05523 ± 0.00324
2177.4	346.32 ± 30.91	0.06075 ± 0.00280
2234.1	401.77 ± 38.83	0.07096 ± 0.00353
2290.7	501.42 ± 40.78	0.06784 ± 0.00366
2347.5	621.88 ± 44.07	0.06635 ± 0.00397
2404.0	576.83 ± 43.31	0.07142 ± 0.00393
2460.8	567.16 ± 45.99	0.07026 ± 0.00414
2517.5	573.19 ± 43.56	0.06829 ± 0.00391
2574.2	589.49 ± 42.81	0.05916 ± 0.00387
2631.0	453.97 ± 34.32	0.07595 ± 0.00308
2687.5	581.15 ± 59.36	0.07417 ± 0.00528
2744.3	480.44 ± 54.11	0.07089 ± 0.00479
2800.9	542.11 ± 44.89	0.06289 ± 0.00398
2857.7	470.46 ± 51.52	0.06325 ± 0.00450
2914.4	541.17 ± 47.23	0.05873 ± 0.00409
2970.9	493.29 ± 53.40	0.06824 ± 0.00460
3027.7	602.71 ± 48.69	0.06008 ± 0.00416

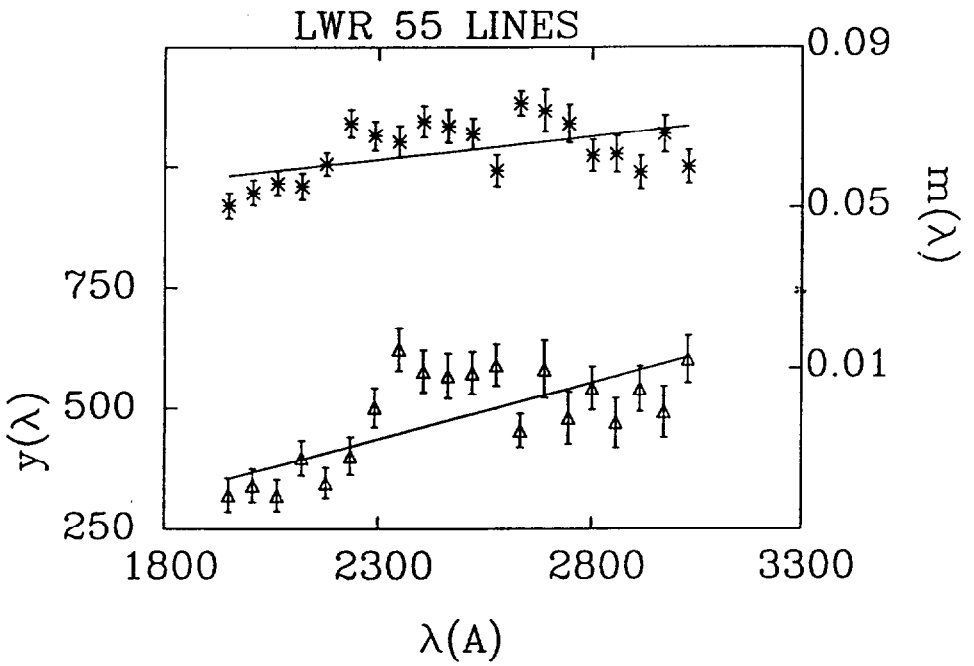

Figure 6 – Plot of σ as a function of fitting parameters $m(\lambda)$ and $b(\lambda)$ for the LWP/55 data.

Table 7

Dependence of Noise on FN and λ

Camera (LBL)	A	B	C	D
SWP (55)	$-3.58 \times 10^{-5} \pm 0.53 \times 10^{-5}$	0.0995 ± 0.0086	-0.265 ± 0.022	589.6 ± 35.5
SWP (110)	$-6.77 \times 10^{-5} \pm 0.83 \times 10^{-5}$	0.171 ± 0.014	-0.202 ± 0.014	427.7 ± 24.4
LWP (55)	$7.29 \times 10^{-5} \pm 0.26 \times 10^{-5}$	0.254 ± 0.007	-0.468 ± 0.016	1571.8 ± 44.9
LWP (110)	$-9.81 \times 10^{-5} \pm 0.03 \times 10^{-5}$	0.333 ± 0.008	-0.315 ± 0.009	1010.9 ± 23.4
LWR (55)	$1.15 \times 10^{-5} \pm 0.03 \times 10^{-5}$	0.035 ± 0.006	0.235 ± 0.028	-104.0 ± 68.9

Table 8

Comparison of our results with those of Kinney *et al.*

Wavelength		1250 Å		1550 Å		1850 Å	
Camera (LBL)	Ref.	b	m	b	m	b	m
SWP (55)	Kinney *et al.*	256.8	0.076	212.1	0.050	93.7	0.028
	Urry *et al.*	258.4	0.055	178.9	0.044	99.4	0.033
SWP (110)	Kinney *et al.*	147.1	0.087	100.8	0.064	44.5	0.035
	Urry *et al.*	175.2	0.086	114.6	0.066	54.0	0.046
Wavelength		2300 Å		2600 Å		2900 Å	
Camera (LBL)	Ref.	b	m	b	m	b	m
LWP (55)	Kinney *et al.*	475.0	0.096	401.0	0.059	239.6	0.038
	Urry *et al.*	495.4	0.086	355.0	0.064	214.6	0.043
LWR (55)	Kinney *et al.*	693.3	0.057	658.5	0.058	661.7	0.058
	Urry *et al.*	436.5	0.061	507.0	0.065	577.5	0.068